



HAL
open science

Noise properties of Pb/Cd-free thick film resistors

Adam Witold Stadler, Andrzej Kolek, Zbigniew Zawiański, Krzysztof Mleczko,
Malgorzata Jakubowska, Konrad Rafal Kielbasiński, Anna Mložniak

► **To cite this version:**

Adam Witold Stadler, Andrzej Kolek, Zbigniew Zawiański, Krzysztof Mleczko, Malgorzata Jakubowska, et al.. Noise properties of Pb/Cd-free thick film resistors. *Journal of Physics D: Applied Physics*, 2010, 43 (26), pp.265401. 10.1088/0022-3727/43/26/265401 . hal-00629953

HAL Id: hal-00629953

<https://hal.science/hal-00629953>

Submitted on 7 Oct 2011

HAL is a multi-disciplinary open access archive for the deposit and dissemination of scientific research documents, whether they are published or not. The documents may come from teaching and research institutions in France or abroad, or from public or private research centers.

L'archive ouverte pluridisciplinaire **HAL**, est destinée au dépôt et à la diffusion de documents scientifiques de niveau recherche, publiés ou non, émanant des établissements d'enseignement et de recherche français ou étrangers, des laboratoires publics ou privés.

Noise properties of Pb/Cd-free thick film resistors

Adam Witold Stadler¹, Andrzej Kolek¹, Zbigniew Zawislak¹, Krzysztof Mleczko¹,
Małgorzata Jakubowska^{2,3}, Konrad Rafał Kielbasiński^{2,4} and Anna Młozniak²

¹Department of Electronics Fundamentals, Rzeszow University of Technology, W.
Pola 2, 35-959 Rzeszow, Poland

²Institute of Electronic Materials Technology, 133 Wolczynska str., Warsaw, 01-919,
Poland

³Warsaw University of Technology, Faculty of Mechatronics, Andrzeja Boboli 8 str.,
Warsaw, Poland

⁴Warsaw University of Technology, Institute of Microelectronics and Optoelectronics,
Koszykowa 75 str., Warsaw, Poland

E-mail: astadler@prz.edu.pl

Abstract. Low-frequency noise spectroscopy has been used to examine noise properties of Pb/Cd-free RuO₂- and CaRuO₃-based thick films screen printed on alumina substrates. Experiments were performed in temperature range 77 - 300 K and frequency range 0.5 – 5000 Hz with multiterminal devices. The measured noise has been recognized as resistance noise that consists of background 1/f noise and components generated by several thermally activated noise sources of different activation energies. The total noise has been composed of the contributions generated in resistive layer and in resistive/conductive layers interface. These noise sources are non-uniformly distributed in the resistor volume. Noise intensity of new-resistive layers has been described by noise parameter, C_{bulk} . Pb/Cd-free layers occurred to be noisier than their Pb-containing counterparts, however the remove of Pb and Cd from resistive composition is hardly responsible for the increase of the noise. In case of RuO₂ layers noise increases most likely due to larger grain size of RuO₂ powder used to prepare resistive pastes. The information about the quality of resistive-to-conductive layers interface occurred to be stored in the values of noise parameter C_{int} . Pb/Cd-free RuO₂-based resistive pastes form well-behaved interfaces with various Ag-based conductive pastes. On the contrary, CaRuO₃-based paste forms bad contacts with AgPd terminations because density of TANSs increases in the interface area.

1. Introduction

Thick film resistors (TFRs) gain a wide variety of applications. Developed by many years, they achieved high quality and are commonly used in both commercial and specialized electronics. Their main features are wide range of sheet resistances, high stability and low temperature coefficient of resistance (TCR). Even the noise figure, for long time considered as not satisfactory, now is suppressed to acceptable level. Materials used in cermet TFRs fabrication are RuO₂ and/or various ruthenates which are the ingredients of resistive pastes and Ag, Au, Pd and Pt which are contained in

conductive pastes used for resistors terminations. Both resistive and conductive pastes are also made of various kinds of glasses that usually contain Pb. Manufacturers optimized their products in order to offer systems of compatible pastes that form well matching resistive-to-conductive film interfaces as well as low ohmic, high reliable joints with conventional Sn/Pb solders. The situation has changed only after RoHS directive was introduced. First, the restrictions for the use of Pb-containing solders forced the manufacturers to workout new conductive pastes able to form good joints with Pb/Cd-free solders. Second, lead has started being eliminated both from conductive and resistive inks [1, 2, 3, 4, 5]. Consequently, recently new pastes have appeared on the market, which are not as well described and optimized as their Pb-containing antecedents.

This paper explores the field of cermet TFRs manufactured with the use of novel materials prepared to fulfill RoHS directive [2]. Several combinations of (i) resistive pastes made of RuO_2 or CaRuO_3 powder and glass of complex composition and (ii) conducting pastes based on Ag, Ag-Pd, or Ag-AgPt-Pd have been used to manufacture TFRs on alumina substrates in high-temperature process. We aim at the description and evaluation of the quality of the interface between resistive and conductive layers that form in these resistors. Our main experimental tool is the low-frequency noise spectroscopy (LFNS) which recently has been proved to be very efficient method for such research [6, 7, 8, 9]. This method enables the estimation of the noise parameters which qualitatively describe the strength of interaction between resistive and conductive layers as well as estimation of the noise index of the resistive layer itself which is also important, as in general there is lack of studies on noise of Pb/Cd-free TFRs especially in a wide range of temperature.

2. Samples

2.1. Geometry

Samples are designed as multiterminal devices. Resistive layer of $L = 15$ mm length and $w = 1$ mm width is terminated by two opposite current contacts and has several lateral voltage probes evenly spaced along both its sides. The advantage of such geometry has been proved in many noise-oriented experiments [8, 10, 11, 12, 13]. The shape of sample TFR and contacts enumeration scheme are shown in the inset of figure 1.

2.2. Materials

The conducting constituent in resistive pastes is either RuO_2 or CaRuO_3 . The mean grain size of RuO_2 powder has been estimated as $d \approx 1 \mu\text{m}$ [14]. The method of digital image processing and analysis was employed to obtain this value. For CaRuO_3 powder, the use of SEM allows the estimation of mean grain size of $d \approx 0.5 \mu\text{m}$. $\text{RuO}_2/\text{CaRuO}_3$ powders are mixed together with Pb/Cd-free glass and ethylcellulose based organic vehicle to give resistive pastes containing 35%/27% of conductive phase by volume. Two types of glass were used. Both of them contain SiO_2 , B_2O_3 , Al_2O_3 , V_2O_5 , and metal oxides: either MgO, CaO, ZnO, Na_2O , K_2O (glass – R16) or BaO (glass – R10). Contacts to resistive films are made from Ag-based pastes. Namely, Ag, Ag-AgPt-Pd, and AgPd pastes were used as listed in table 1. All conductive and resistive pastes were developed as Pb/Cd-free materials according to RoHS directive [15, 16, 17], and were produced in the Institute of Electronic Materials Technology (ITME), Warsaw, Poland. In table 1 samples used in this study, their description, details of fabrication and some features are collected.

Table 1. Samples labeling and details.

sample	Resistive paste		contacts		thickness, μm	R_{sq} , $\text{k}\Omega$	ρ , Ωcm	size effect
	Conducting constituent	glass	Conductive constituent	Paste				
P-121 Sz R-16-65 RuO_2	$\text{RuO}_2 - 35\%$	R-16	Ag	P-121	21.2	4.29	9.09	1.028
P-511 Sz R-16-65 RuO_2	$\text{RuO}_2 - 35\%$	R-16	Ag-AgPt-Pd	P-511	20.4	4.28	8.77	1.028

P-202 Sz R-16-65 RuO ₂	RuO ₂ – 35%	R-16	AgPd	P-202	20.8	4.24	8.83	1.024
P-202 Sz R-10-73,5 CaRuO ₃	CaRuO ₃ – 26.5%	R-10	AgPd	P-202	20.7	17.53	36	1.035

2.3. Printing and firing

Resistive pastes were printed onto alumina substrates through 200 mesh screen. After drying in 120 °C for 15 min., films were fired in a tunnel furnace gaining the final thickness of ~ 20 μm (figure 1). The process of firing followed a suitable temperature profile with peak temperature at 850 °C lasting 10 minutes. Contacts to the films were made of conductive pastes in a very similar process. They were deposited onto substrates prior to resistive films printing.

2.4. Selection and entry tests

Several tens of resistors in 6 series have been manufactured. They were then aged in temperature 125 °C for 100 hours. The drift of the resistance of RuO₂-based resistors was less than 0.1%, whereas for CaRuO₃-based resistors it usually exceeded 1%. In fact, out of 3 series of CaRuO₃ based resistors, only those with AgPd contacts survived the ageing, maintaining reasonable long-term stability. Therefore, only samples from this CaRuO₃-based series as well as samples from all 3 RuO₂-based series were used in noise measurements. For each series, one pair of samples that match best their resistance at room temperature was selected for further studies. Total resistance between terminations 1 and 7 ($R \equiv R_{1-7} = V_{1-7}/I$, where I is biasing current and V_{1-7} is the voltage between terminations 1-7) was used as a matching criterion. For all selected samples, voltage distribution along resistive layer was measured (figure 1) to evaluate size effect [8], and estimate sheet resistance R_{sq} . Size effect was calculated as the ratio of average resistance per square, R_{1-7}/L , and “bulk” sheet resistance $R_{sq} = V_{2-6}/(L_{2-6}I)$, L_{2-6} is the length of the sector 2-6 (i.e. the part of the main film that extend between contacts 2 and 6) and V_{2-6} is the voltage across this sector. It stems from the data gathered in table 1 that for our Pb/Cd-free TFRs size effect is negligible. The thickness of resistive film in-between side probes was measured directly using Vistronik C1 meter. Average film thickness was then used to calculate film resistivity ρ .

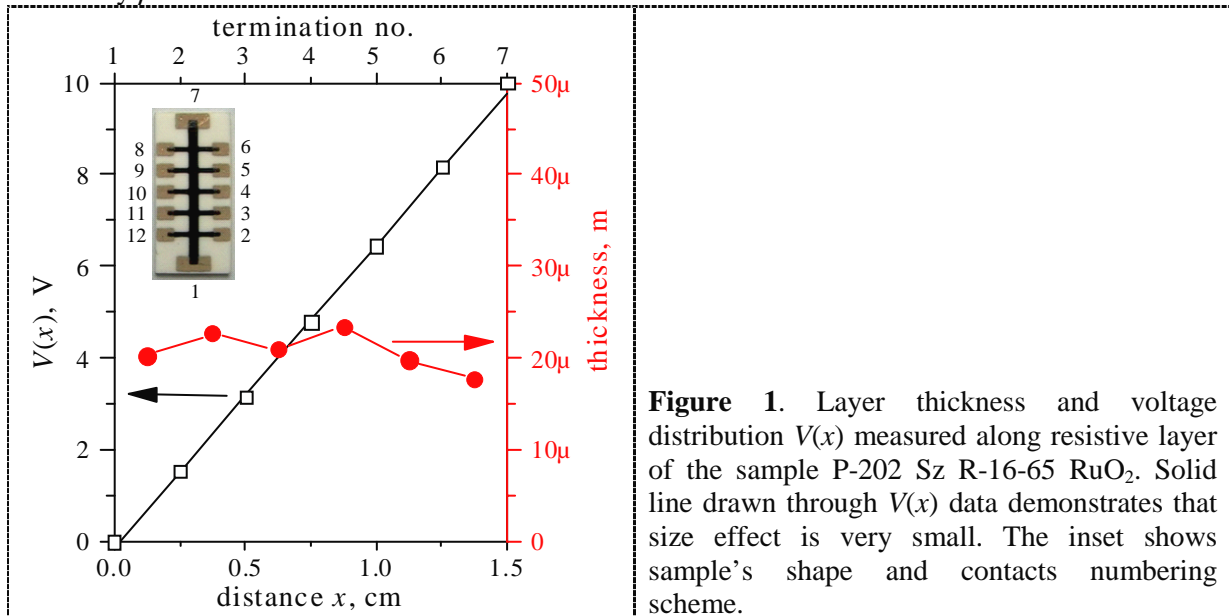


Figure 1. Layer thickness and voltage distribution $V(x)$ measured along resistive layer of the sample P-202 Sz R-16-65 RuO₂. Solid line drawn through $V(x)$ data demonstrates that size effect is very small. The inset shows sample's shape and contacts numbering scheme.

3. Noise measurements

3.1. Experimental setup

Low-frequency noise has been measured in dc bridge configuration (see figure 2). A selected pair of samples was placed in the bottom arms of the bridge and biased through load resistors of much larger resistance. Only the samples and the calibrated temperature sensor (Pt-100 RTD) were inserted into LN cryostat and subjected to cooling. The voltages from the bridge diagonal and sub-diagonals were conditioned in ac-coupled low-noise differential preamplifiers and low-pass filtered. Noise Signal Analyzer [18] was used to manage experiment and calculate power spectral densities (PSDs) of measured voltages. Additional equipment shown in figure 2 is involved to monitor actual temperature and record bias voltage and current. All is controlled via GPIB interface.

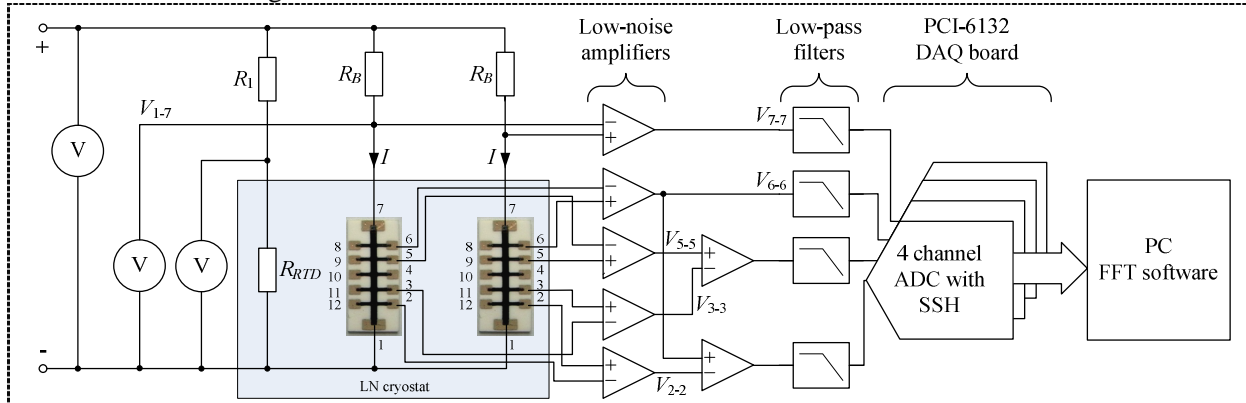


Figure 2. Measurement setup for low-frequency noise spectroscopy.

Noise Signal Analyzer calculates the cross-power spectra of the voltages V_{X-Y} acquired from-between a certain pair of voltage probes and the voltage V_{7-7} from-between the terminations No. 7. As the V_{2-2} contains a part of V_{7-7} , their cross-PSD refers to the fluctuations originated from these sectors of the resistors, which give contribution to both voltages. This is illustrated in figure 3a: PSD S_{2-2} measured (for different bias, $V \equiv V_{1-7} = 7.8$ V and $V = 0$) between the terminations No. 2 refers to the noise signal generated in (i) contact No. 1/main film interfaces, (ii) sectors 1-2 of the main resistive film, (iii) side legs No. 2 that include resistive film lead and contact No. 2. On the contrary cross-PSD of voltages V_{2-2} and V_{7-7} refers only to the signal generated in sectors 1-2 of the main film, so that $S_{2-2} > S_{2-2,7-7}$. As shown in figure 3a the difference is not much for biased samples as in this case the signal of component (ii) is much greater than the other two. However, the difference becomes quite large for $V = 0$, when all three components give signals of the same order.

In the experiment, noise generated in successive sectors of the resistor was of interest. Measurements have been made for sectors 1-7 (whole resistor), 1-6, 2-6, 3-5. Its power spectral density, S_V was measured with the cross-correlation method as described above. Of them, only the sectors 2-6 and 3-5 have spectra that are free from noises generated in current and voltage contacts. Unlike these two, spectra acquired for sectors 1-7 include noise generated in both upper and lower current contacts, whereas spectra for sectors 1-6 contain noise generated only in lower current taps.

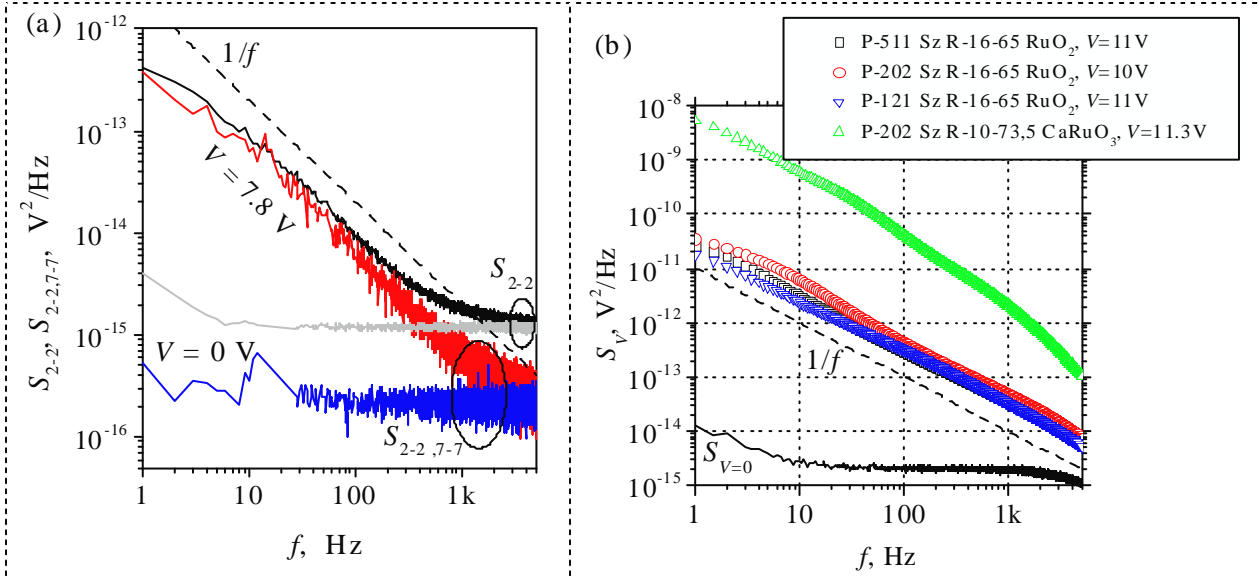


Figure 3. (a) PSD of voltage fluctuations measured directly at contacts 2-2 and cross-PSD measured for voltages $V_{2,2}$ and $V_{7,7}$. Both were measured with bias ($V = 7.8$ V) and with no bias ($V = 0$) (b) Noise spectra measured at room temperature (symbols). Solid line shows background noise for the sample P-121 Sz R-16-65 RuO_2 . In (a) and (b) dashed line shows the spectrum of pure $1/f$ noise.

As shown in figure 3a noise spectra were measured for non-zero bias voltages (S_V) as well as with no bias (background noise $S_{V=0}$). Excess noise was then calculated as $S_{V_{ex}}(f) = S_V(f) - S_{V=0}(f)$. Examples of the measured spectra are shown in figure 3b: $1/f$ noise contributes most to non-equilibrium $S_V(f)$ dependence. Background noise in case of cross-correlation measurements is dominated mainly by thermal noise of the resistors. Only for the spectra measured for the whole resistor, it is described both by the source resistance and by the amplifier equivalent noise resistance, which is ≈ 1.1 k Ω . The spectrum $S_{V=0}$ shown in figure 3b refers to this case. As shown, $1/f$ background noise dominates only below 10 Hz and is much lower than the noise of the biased samples.

All signals are sampled simultaneously and spectra are calculated in real time in a frequency range from 0.5 Hz to 5 kHz with 0.5 Hz resolution employing 2^{19} point FFT. Only low-frequency part 0.5 – 5000 Hz is recorded for further processing.

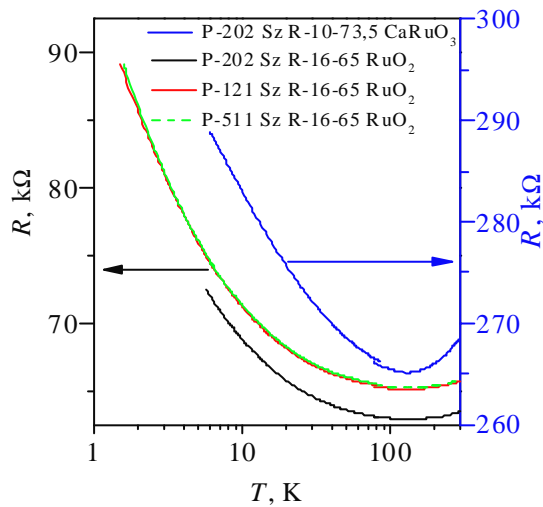
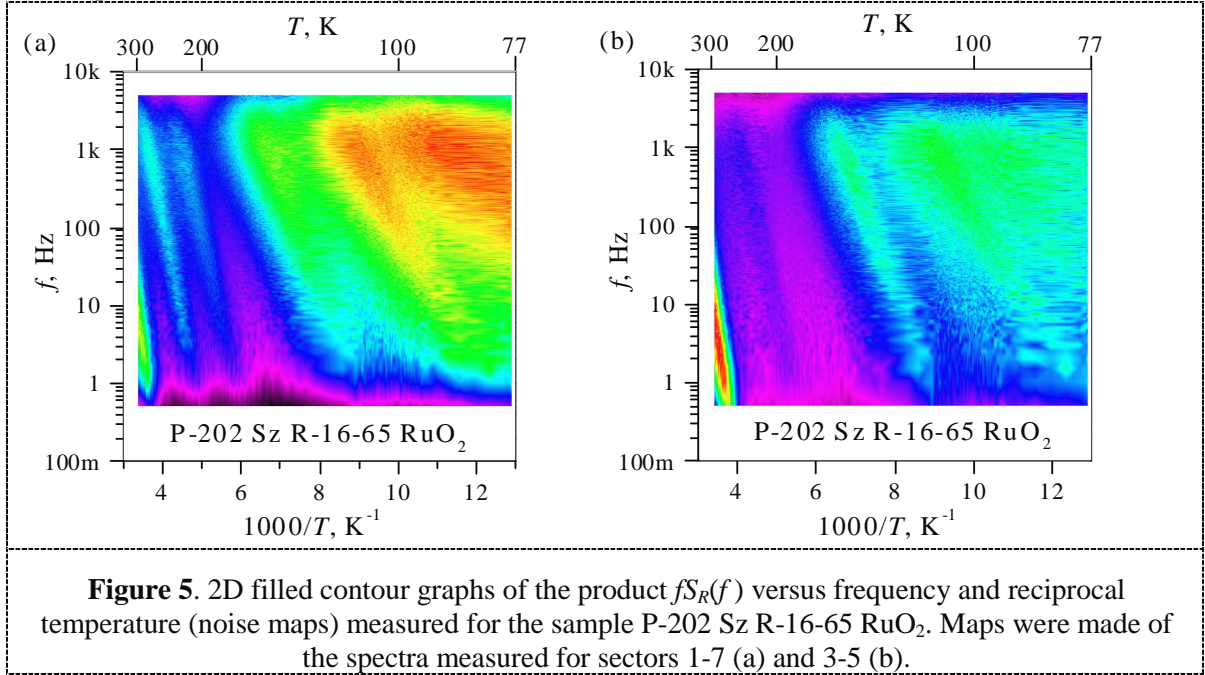


Figure 4. Resistance R vs. temperature. In the range 77 – 300 K, resistances and noise spectra were measured simultaneously.

3.2. Low-frequency noise spectroscopy

Low-frequency noise spectroscopy was used in the investigations of e.g. semiconductor materials and devices [19], UV detectors [20], gas sensors [21] and TFRs [6, 7, 8, 10, 11]. The method examines the evolution of low-frequency noise spectrum as a function of temperature. In our experiment, noise spectra were measured as a function of slowly ramping temperature in the range 77 – 300 K. Noise data are presented in the form of noise maps i.e. 2D contour graphs of the product $fS_R(f)$ versus frequency and reciprocal temperature [7, 10, 11]. Sample noise maps are shown in figure 5. During these measurements, the resistance R of the samples was also recorded. R vs. T curves obtained in these experiments are shown in figure 4. Below 77 K, $R(T)$ was measured in helium cryostat.



4. Results and discussion

4.1. Resistance fluctuations

The dependence of noise intensity on the excitation voltage (or current) is one of major tests for noise identification. Since noise spectra may include components like $1/f$ and/or Lorentzians, it is desirable to perform this test with respect to noise power in different frequency bands. Sample results are illustrated in figure 6 where the product $fS_{V_{ex}}(f)$ averaged in frequency bands (decades) is plotted versus the bias voltage. Lines, if drawn through the points, would have the slope of 2. Thus, all parts of the spectrum depend linearly on excitation voltage square, which is the sign that all components of the noise originate from resistance fluctuations (resistance noise) [22]. PSD of these fluctuations can be calculated as $S_R(f) = S_{V_{ex}}(f)/I^2$. This quantity is bias independent, and so the spectra $S_R(f)$ are used in LFNS. Physical mechanisms that can lead to resistance fluctuations in TFRs were discussed in ref. [7]. It stems from that discussion that fluctuating mobility is responsible for these fluctuations.

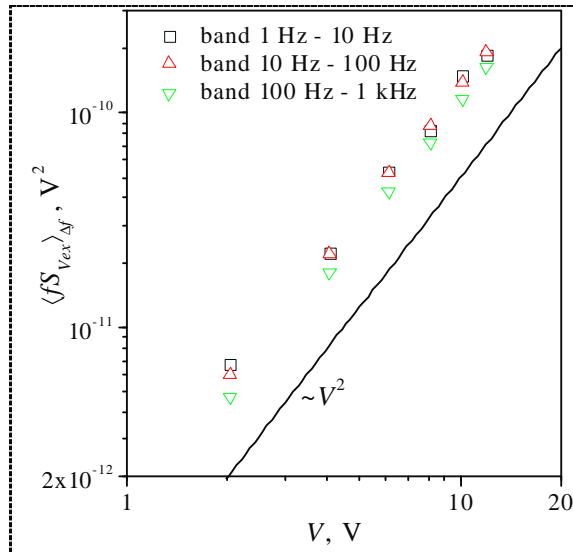


Figure 6. The product $fS_{V_{ex}}(f)$ averaged $\langle \rangle$ over frequency decades versus the bias voltage. Solid line indicates proportionality to V^2 . The measurements were performed at room temperature for sample P-121 Sz R-16-65 RuO₂.

4.2. Thermally activated noise sources

The use of LFNS makes possible identification of thermally activated noise sources (TANSs) in the measured noise signal and estimation of their activation energy E_a . On the maps like these in figure 5, TANSs appear as the streaks [7, 23] whereas smooth surface between the streaks refers to pure $1/f$ noise. The value of E_a can be calculated from the slope of the streak [6, 23]. Each value of the activation energy is associated with two-state system localized in grain boundaries and/or in the glass [7]. Transitions in these systems are thermally activated. They couple to (modulate) the local resistances. Only those that modulate critical resistances in the percolation path [24] contribute significantly to the overall resistance and can be detected in noise measurements. Therefore merely few activation energies are observed for individual samples. The discrete set of their values differs from sample to sample but all values of E_a found in this work, fall into the range 0.083 – 0.74 eV. These values are a bit lower than the value $E_a \approx 1.15$ eV found in ref. [25], but fit well within the range of activation energies found in refs. [7, 10, 26] for Pb-containing TFRs. For definiteness, one should note, however, that in ref. [25] measurements cover temperature range up to 800 K, where different TANSs are active.

Apart from detection of TANSs and their activation energies, noise maps give more informative view on fluctuating phenomena that take place in TFRs. Noise maps shown in figure 5 refer to different sector of the same resistor. The map of figure 5a refers to resistance fluctuations measured for sectors 1-7 whereas the map of figure 5b refers to internal sector 3-5. Data on both maps were gathered simultaneously. As different streaks appear on figures 5a and 5b it is obvious that intensity and number of TANSs vary from sector to sector. In other words, TANSs (and the corresponding two-state systems) are randomly distributed inside the resistor.

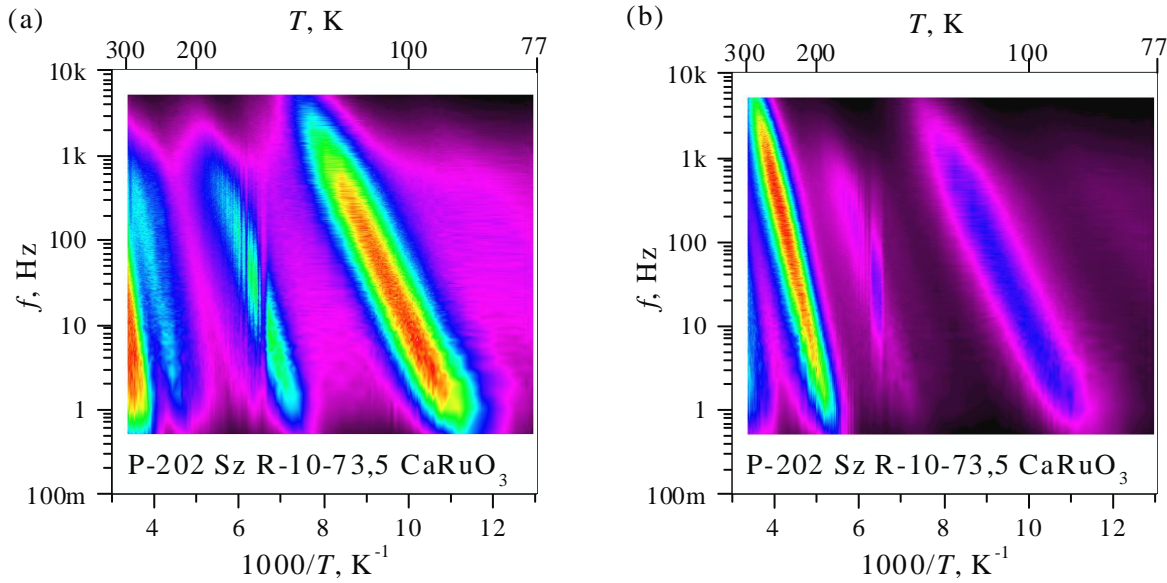


Figure 7. Noise maps for sample P-202 Sz R-10-73,5 CaRuO₃, measured for sector 1-7 in two different experiments.

Another interesting phenomenon observed on the noise maps is spectra switching. It vertically “cuts” the maps and divides the streaks into separate pieces (see figure 7). Physically it means that in a certain temperature TANS is accidentally turned on/off in a sharp manner. Possible reasons for this process were discussed in refs. [8, 10] and involve dynamic current redistribution due to stress relaxation, and/or interacting fluctuators. Briefly, when current is redistributed (topology of percolation cluster changes) certain TANSs become more distant from the percolation network, so they no longer can modulate critical resistances in this network and no longer can be observed as the fluctuations at the overall resistance. In our experiments spectra switching has not been observed for RuO₂-based TFRs. For CaRuO₃-based TFRs series, switching of the spectra was observed in temperature range 150 – 160 K. It is interesting that in different cooling-heating cycles the switching of the spectra always took place in the same temperature range. As shown in figure 7, in different experiments TANS of different activation energy and intensity appears. This means that process of switching can turn on/off TANS also in time scale that exceeds single experiment; that is, it is non-stationary in this time scale.

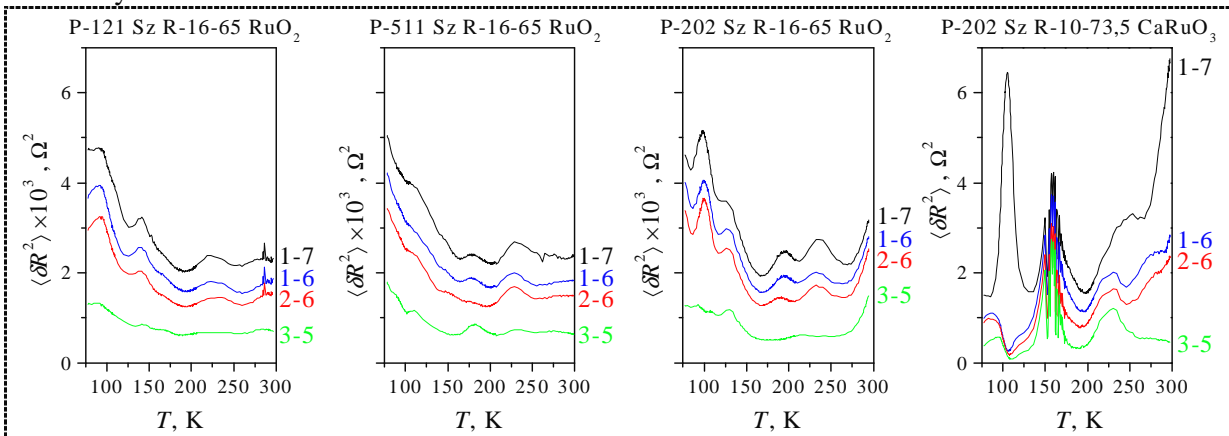


Figure 8. The power of resistance fluctuations $\langle \delta R^2 \rangle$ in band 10 – 100 Hz vs. temperature for different sectors of the samples. All three graphs for RuO₂-based TFRs have identical vertical scale. CaRuO₃-based TFR has the values of $\langle \delta R^2 \rangle$ larger by three orders of magnitude.

4.3. Noise scaling and decomposition

The intensity of all noise sources localized in a resistor's sector is given by the power of its resistance fluctuations $\langle \delta R^2 \rangle$. Exemplary plots of $\langle \delta R^2 \rangle$ versus temperature are shown in figure 8. As noise maps are sample-dependent, so are the plots $\langle \delta R^2 \rangle(T)$. That is why the plots for RuO₂ based TFRs in figure 8 are different: different contacts are hardly responsible for these differences. For CaRuO₃-based sample the number of TANSs, and intensity of the noise they generate, increase in the sector close to the upper (No. 7) resistor termination. For the remaining samples the density of TANS in a resistor volume is more or less homogeneous. To prove it the integral measure of noise [8]:

$$s \equiv \frac{1}{T_2 - T_1} \int_{T_1}^{T_2} \int_{f_l}^{f_u} S_R(f, T) df dT, \quad (1)$$

was scaled versus sector size. The integration in equation (1) should be over the surface as broad as possible. However, the measurement conditions describe the frequency and temperature limits of the integral: the frequency band 10 – 100 Hz, has been chosen in order to omit (i) distortion of the spectra in low-frequency limit caused by temperature drift, (ii) overlapping 1/f resistance noise by thermal noise in high-frequency limit [8]. Temperature range 77 – 300 K was used due to the cryostat capabilities. Plotting the integral s versus the sector size enables decomposition of the measured noise into bulk and contact components. The approach is illustrated in figure 9 where the plots for the samples P-202 Sz R-16-65 RuO₂ and P-202 Sz R-10-73,5 CaRuO₃ are shown. The points referred to the internal sectors of the resistor very tightly follow straight lines that start at the plot origin. Such linear increase of noise intensity is expected for spatially uncorrelated noise sources. The slope of the line gives bulk noise per square s_{sq} that can be used to calculate dimension-independent bulk noise intensity $C_{bulk} \equiv s_{sq}/R_{sq}^2 \times \Omega_{sq}$, where Ω_{sq} is the square volume. Parameter C_{bulk} occurred to be very helpful when comparing noise properties of different materials [8, 27, 28].

The noise generated in the interfaces of both current contacts can be evaluated as a difference between noise intensity measured for whole resistor, s_{1-7} , and extrapolated bulk noise $s_{bulk} = L/w \times s_{sq}$. Namely $2s_{int} = s_{1-7} - s_{bulk}$. The “quality” of the interface is described by contact-geometry-independent parameter, $C_{int} \equiv ws_{int}/s_{sq}$ [8]. Numerically, its value is the length of hypothetical resistive film, which would have the noise intensity equal the intensity of the interface noise. Parameters C_{bulk} and C_{int} have been calculated and are collected in table 2.

Due to the non-stationary behavior observed for CaRuO₃-based samples, numerical values of integral s obtained for this resistor in different experiments are different. This explains scattering in the values of s observed for this sample in figure 9. The scattering is the largest for the value of s_{1-7} what means that most non-stationary switchings occur in the interfaces. For other samples, the values of s are not scattered. As they were obtained for different bias voltages this is in line with the conclusion that stationary resistance fluctuations are the origin of the noise.

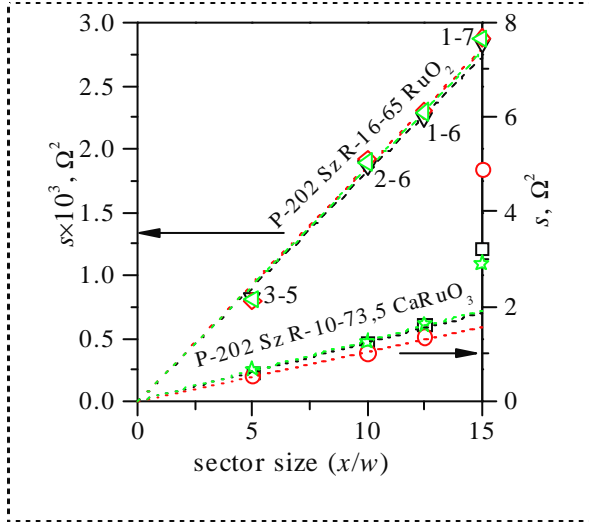


Figure 9. The integral s vs. sector size (expressed in the number of squares in the sector). Different symbols refer to different measurements (cool-warm cycles) with different bias voltages. Sectors are labelled near RuO_2 series.

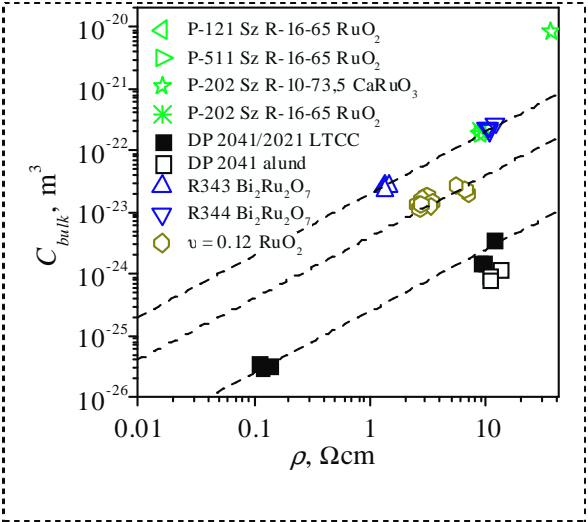


Figure 10. Comparison of the bulk noise of various TFRs. Lines are the plots of relation $C_{bulk} = K'\rho$ with different values of the coefficient K' .

Table 2. Noise parameters of Pb/Cd-free TFRs.

sample	P-121 Sz R-16-65 RuO_2	P-511 Sz R-16-65 RuO_2	P-202 Sz R-16-65 RuO_2	P-202 Sz R-10-73,5 CaRuO_3
$C_{bulk} \times 10^{24}, \text{m}^3$	198	190	215	8571
C_{int}, mm	0.56	0.77	0.25	3.92

4.4. Noise of resistive films

It has been shown by means of theoretical considerations [29, 30] and verified experimentally [29, 31], that bulk noise of TFRs is proportional to resistivity ρ , $C_{bulk} = K'\rho$, when resistivity is changed by the content of conductive constituent of the resistive paste. As in this study, samples with different $\text{RuO}_2/\text{CaRuO}_3$ content are not available we refer to our previous work of ref. [8] in order to compare bulk noise of Pb/Cd-free compositions with its Pb-containing antecedents. In figure 10, data for TFRs studied in ref. [8] have been plotted together with the current data, all as C_{bulk} vs. resistivity. One can see that noise of CaRuO_3 films is the largest also when compared to non Pb/Cd-free TFRs. Note, however, that resistivity of these films is relatively high.

Regarding Pb/Cd-free RuO_2 -based resistive films, experimental points in figure 10 lie on the line with $K' = 2 \times 10^{-9} \mu\text{m}^2/\Omega$ which is almost an order of magnitude larger than the value $K' = 4 \times 10^{-10} \mu\text{m}^2/\Omega$ found in ref. [8] for Pb-containing RuO_2 films. The question appears for the reason of such large discrepancy. In our opinion the reason for this is the difference in RuO_2 grain size in resistive films studied in ref. [8] where $d \approx 10 \text{ nm}$ and in this work, where $d \approx 1 \mu\text{m}$. Although there are only few studies concerning the influence of grain size on noise of TFR [29, 30, 31, 32, 33], it has been rather argued that increase in the grain size results in both larger resistivity [31, 32, 33] and bulk noise. From theoretical point of view the relations $\rho \sim d$, $C_{bulk} \sim d^3$, and thus $C_{bulk} \sim \rho^3$ are expected when ρ is driven solely by the grain size of the conductive powder [30, 31]. Experimentally, the increase of sheet resistance with conductive constituent grain size was observed, e.g. in refs. [29, 30, 31, 32, 33]. Much less frequent are noise versus grain size measurements. For $\text{Bi}_2\text{Ru}_2\text{O}_7$ -based films the relation $C_{bulk} \sim R_{sq}^{2.4}$ was found in ref. [31]. In refs [33] and [34] increase of the noise intensity with increasing grain size was observed for RuO_2 -based TFRs. Obviously, our data are not rich enough to definitely and quantitatively verify the hypothesis, but it seems that increase in the value of C_{bulk} observed for our

Pb/Cd-free RuO₂ films is caused by the increase of conductive constituent grain size rather than by Pb-remove.

4.5. Interface noise

Parameter C_{int} can be used to evaluate the usefulness of various combinations of resistive and conductive pastes in forming well-behaved resistive/conductive films interfaces. Relatively large value of C_{int} indicates that the contact significantly contributes to the noise of the resistor, degrading performance characteristics of the device. Analyzing the values of C_{int} gathered in table 2, one can conclude that Pb/Cd-free RuO₂ films form well-behaved contacts made of various Ag-based conductive pastes. On the other hand, the interface of CaRuO₃-based sample is poor: CaRuO₃ films should not be terminated with AgPd contacts.

5. Summary

LFNS technique has been applied to study noise properties and evaluate systems of materials to be used in RoHS compliant TFRs technology. Four samples made of different combinations of Pb/Cd-free resistive and conductive pastes have been examined in temperature range 77 – 300 K. Two basic components of low-frequency noise have been detected. Namely 1/f noise and TANSs, each of them is resistance noise. In every sample, several TANSs have been observed. Their activation energies seem to be resistor rather than material specific. It has occurred that TANSs are non-uniformly distributed in the resistor volume.

Pb/Cd-free RuO₂-based resistive pastes form well-behaved interfaces with various Ag-based conductive pastes. On the contrary, CaRuO₃-based paste forms bad contacts with AgPd terminations because density of TANSs increases in the interface area. This knowledge will certainly be helpful in further optimization of materials systems used in the fabrication of Pb/Cd-free low-noise, stable and reliable TFRs. It could have been gained in spite that in all our samples the size effect, estimated from ordinary resistance measurements (table 1), was negligible. We came to these conclusions due to the advantages of the research method we used. The information about the quality of resistive-to-conductive layers interface occurred to be stored in the values of noise parameter C_{int} .

Noise intensity of new-resistive layers has been described by another noise parameter, C_{bulk} . Its values have been calculated and compared with those available in the literature [8]. Pb/Cd-free layers occurred to be noisier than their Pb-containing counterparts, however the remove of Pb and Cd from resistive composition is hardly responsible for the increase of the noise. Although for CaRuO₃ layers noise data are not available at all, in case of RuO₂ layers noise increases most likely due to larger grain size of RuO₂ powder used to prepare resistive pastes.

The values of parameters C_{int} and/or C_{bulk} contribute to noise index of a resistor – an important parameter for its applications and valuable indicator of its reliability, long-term drift and lifetime [35] and efficient tool in failure prediction of electron devices and circuits [36, 37,38].

The region of low temperatures explored in the paper is of special interest as since 1970's TFRs enter the field of cryogenics, where they are used as temperature sensors [39, 40, 41, 42,43]. They exhibit large sensitivity to temperature changes due to the resistance sharply increasing below several K. Physical reasons for this increase is unknown. Thermally activated tunneling [44], fluctuation induced tunneling [45,46], conduction in a narrow band [47], variable range hopping (VRH) [48,49], space charge limited transport [50], emissions over graded barriers [46], and weak localization [51], are considered as transport mechanisms – none is able to fully explain the feature. Our present results add the contribution to the practical aspect of the field: Pb/Cd-free compositions can be used as thermo-sensing layers in cryogenic RTD's. From figure 4 one can deduce that below 10 K these compositions maintain high sensitivity to temperature changes.

Acknowledgments

The work has been supported by the Polish Ministry of Science and Higher Education through grant no N N515 341836 .

References

- [1] Morten B Ruffi G Sirotti F Tombesi A Moro L and Akomolafe T 1991 Lead-free ruthenium-based thick-film resistors: a study of model systems *Journal of Materials Science: Materials In Electronics* **2** 46-53
- [2] Jakubowska M 2008 Thick Film Materials - Achievements and Trends in Development *Proc. of 32nd Int. Conf. of IMAPS - CPMT IEEE* (Poland, Pułtusk)
- [3] Prudenziati M Zanardi F Morten B and Gualtieri A F 2002 Lead-free thick film resistors: an explorative investigation *Journal of Materials Science-Materials in Electronics* **13** 31-7
- [4] Rane S Prudenziati M Morten B Golonka L Dziedzic A 2005 Structural and electrical properties of perovskite ruthenate-based lead-free thick film resistors on alumina and LTCC *Journal of Materials Science-Materials in Electronics* **16** (10) 687-691
- [5] Maeder T Jacq C Grimaldi C and Ryser P 2009 Lead-free low-firing thick-film resistors based on bismuth glasses and ruthenium oxide *Proc. of 33rd Int. Conf. of IMAPS Poland Chapter* (Poland, Gliwice), pp. 222-229
- [6] Kolek A Stadler AW and Zawislak Z 2006 Noise spectroscopy of thick resistive-conductive film interface *Proc. of 30th Int. Conf. of IMAPS Poland Chapter* (Kraków, Poland)
- [7] Kolek A Stadler AW Ptak P Zawislak Z Mleczek K Szałański P and Żak D 2007 Low-frequency 1/f noise of RuO₂-glass thick resistive films *J. Appl. Phys.* **102** 103718
- [8] Mleczek K Zawislak Z Stadler AW Kolek A Dziedzic A and Cichosz J 2008 Evaluation of conductive-to-resistive layers interaction in thick-film resistors *Microel. Reliab.* **48** 881
- [9] Vandamme L K J and Van Kemenade A J 1997 Resistance noise measurement: A better diagnostic tool to detect stress and current induced degradation *Microel. Reliab.* **37** 87
- [10] Kolek A Stadler A W Zawislak Z Mleczek K and Dziedzic A 2008 Noise and switching phenomena in thick-film resistors *J. Phys. D: Appl. Phys.* **41** 025303
- [11] Kolek A Stadler A W and Zawislak Z 2009 Spatial distribution of noise sources in thick-film resistors *AIP Conference Proceedings* **1129** 157
- [12] Rhee J G and Chen T M 1978 Contact noise in thick film resistors *Solid. State Technol.* **29** 59
- [13] Masoero A Morten B Prudenziati M and Stepanescu A 1990 An improved technique of measuring the contact noise in thick film resistors *Proc. of 10th Int. Conf. On Noise in Physical Systems* (Budapest, Hungary) p 561
- [14] Kiełbasiński K Młóżniak A and Jakubowska M 2009 Vanadium Oxide as a Devitrification Exhibitor in Lead-free Glass for Environmental Friendly Thick Film Resistors *Proc. 33rd Int. Conf. of IMAPS Poland Chapter* (Pszczyna-Gliwice, Poland) p 175 – 178
- [15] Jakubowska M Kalenik J Kiełbasiński K and Młóżniak A 2007 Electrical properties of new lead-free thick film resistors *Proc 31st Int. Conf. of IMAPS Poland Chapter* (Poland, Rzeszów – Krasieczyn) p 323 – 6
- [16] Kiełbasiński K Młóżniak A and Jakubowska M 2008 High ohm eco-friendly resistors in thick film technology *Proc 32nd Int. Conf. of IMAPS Poland Chapter* (Poland, Warszawa-Pułtusk)
- [17] Jakubowska M Kiełbasiński K Młóżniak A Wyżkiewicz I and Zwierkowska E 2008 Lead free thick film materials *Monographies of Tele & Radio Research Institute* (Warsaw, Poland) **1** 87
- [18] Stadler A W 2007 Noise signal analyzer for multi-terminal devices *Proc 31st Int. Conf. of IMAPS Poland Chapter* (Poland, Rzeszów – Krasieczyn) p 413
- [19] Jones B K 1991 Low-frequency noise spectroscopy *IEEE trans. electron devices* **41** 2188
- [20] Ćwirko R Bielecki Z Ćwirko J and Dobrzanski L 2006 Low-frequency noises as a tool for UV detector characterisation *Opto-Electron. Rev.* **14** 155

- [21] Seguin J L, Gomri S, Guerin J and Aguir K 2007 Bases of Noise Spectroscopy for Enhancing Metallic Oxide Gas Sensors Selectivity *Science and technology of chemiresistor gas sensors* ed Aswal D K, Gupta S K (Nova Publishers) p 351
- [22] Hooge F N, Kleinpenning T G M and Vandamme L K J 1981 Experimental studies on 1/f noise *Rep. Prog. Phys.* **44** 479-532
- [23] Stadler A W, Kolek A and Zawislak Z 2005 Thermally Activated Noise Sources in Thick Film Resistors of RuO₂ and Glass *Proc. 28th Int. Spring Seminar on Electronics Technol.* (Wiener Neustadt, Austria) p 358 – 363
- [24] Shklovskii B I and Efros A L 1984 *Electronic Properties of Doped Semiconductors* (Berlin: Springer Verlag).
- [25] Pellegrini B, Saletti R, Terreni P and Prudenziati M 1983 1/f^t noise in thick-film resistors as an effect of tunnel and thermally activated emissions, from measures versus frequency and temperature *Phys. Rev.* **B 27** 1233
- [26] Kolek A, Stadler A, Zawislak Z, Mleczo K, Ptak P, Žak D and Szałański P 2007 Change of Coupling Mechanism in the Low-Frequency Noise of RuO₂-Glass Films *AIP Conf. Proc.* **922** 273 – 6
- [27] Kolek A, Ptak P and Dziedzic A 2003 Noise characteristics of resistors buried in low-temperature co-fired ceramics *J Phys D* **36** 1009
- [28] Vandamme L K J and Casier H J 2004 The 1/f noise versus sheet resistance in poly-Si is similar to poly-SiGe resistors and Au-layers *Proc 34th European solid-state device research conf* (Leuven, Belgium) p 21
- [29] Vandamme L K J 1977 Criteria of Low-Noise Thick-Film Resistors *ElectroComp. Sci. Technol.* **4** 171
- [30] Wolf M, Müller F and Hemschik H 1985 Comment on the dependence of R_□ and current noise on grain size in thick film resistors—TFR's *Active and Passive Elec. Comp.* **12** 59
- [31] Müller F and Wolf M 1988 Dependence of the Sheet Resistivity and Current Noise Behaviour of the Grain Size and Volume Fraction of Conducting Material in Thick-Film Resistors Experiments *Active and Passive Elec. Comp.* **13** 1
- [32] Rao Y S 2007 Studies on electrical properties of polymer thick film resistors *Microelectron Int.* **24/1** 8
- [33] Tamborin M, Piccinini S, Prudenziati M and Morten B 1997 Piezoresistive properties of RuO₂-based thick-film resistors: the effect of RuO₂ grain size *Sensors and Actuators A* **58** 159
- [34] Inokuma T, Taketa Y and Haradome M 1985 Conductive and Insulative Particle Size Effects on the Electrical Properties of RuO₂ Thick-Film Resistors *IEEE Trans. CHMT* **8** 372
- [35] Rocak D, Belavic D, Hrovat M, Sikula J, Koptavy B, Pavelka J and Sedlakova V 2001 Low-frequency noise of thick-film resistors as quality and reliability indicator *Microelectron. Reliab.* **41** 531 – 42
- [36] Jevtić M M 1995 Noise as a diagnostic and prediction tool in reliability physics *Microelectron. Reliab.* **35** 455–77
- [37] Jevtić M M, Mrak I and Stanimirović Z 1999 Thick-film quality indicator based on noise index measurements *Microelectron. Reliab.* **30** 1255-9
- [38] Jevtić M M, Stanimirović Z and Stanimirović I 2001 Evaluation of thick-film resistor structural parameters based on noise index measurements *Microelectron. Reliab.* **41** 59-66
- [39] Willekers R W, Mathu F, Meijer H C, Postma H 1990 Thick film thermometers with predictable R-T characteristics and very low magnetoresistance below 1 K *Cryogenics* **30** 351-355
- [40] Bat'ko I, Flachbart K, Somora M and Vanický D 1995 Design of RuO₂-based thermometers for the millikelvin temperature range *Cryogenics* **35** 105-108
- [41] Goodrich R G, Hall D, Palm E and Murphy T 1998 Magnetoresistance below 1 K and temperature cycling of ruthenium oxide-bismuth ruthenate cryogenic thermometers *Cryogenics* **38** 221-5
- [42] Watanabe M, Morishita M and Ootuka Y 2001 Magnetoresistance of RuO₂-based resistance

- thermometers below 0.3 K *Cryogenics* **41** 143-148
- [43] Ptak P Kolek A Zawiślak Z Stadler A W and Mleczko K 2005 Noise resolution of RuO₂-based resistance thermometers *Rev. Sci. Instrum.* **76** 014901
- [44] Pike G E and Seager C H 1977 Electrical properties and conduction mechanisms of Ru-based thick-film (cermet) resistors *J. Appl. Phys.* **48** 5152-69
- [45] Sheng P Sichel E K and Gittleman J I 1978 Fluctuation-Induced Tunneling Conduction in Carbon-Polyvinylchloride Composites *Phys. Rev. Lett.* **40** 1197-1200
- [46] Flachbart K Pavlik V Tomasovicova N Adkins C J, Somora M Lieb J and Eska G 1998 RuO₂-based Low Temperature Sensors with "Tuned" Resistivity Dependencies *Phys. Stat. Solidi (b)* **205** 399-404
- [47] Hill R 1980 Electrical transport in thick film resistors *Electrocomp. Sci. Technol.* **6** 141-5
- [48] Prudenziati M 1979 On the temperature coefficient of resistivity in thick-film resistors and the percolation model *Alta Frequenza* **XLVI** 147 E-287-8
- [49] Affronte M, Campani M Piccinini S Tamborin M Morten B Prudenziati M Laborde O 1997 Low temperature electronic transport in RuO₂-based cermet resistors *J. Low Temp. Phys.* **109** 461-75
- [50] Vest R W 1975 Conduction mechanisms in thick film microcircuits, Final Technical Report, ARPA Order Number 1642
- [51] Affronte M Campani M Morten B Prudenziati M Laborde O 1998 Magnetoresistance of RuO₂ - based thick film resistors *J. Low Temp. Phys.* **112** 355-71

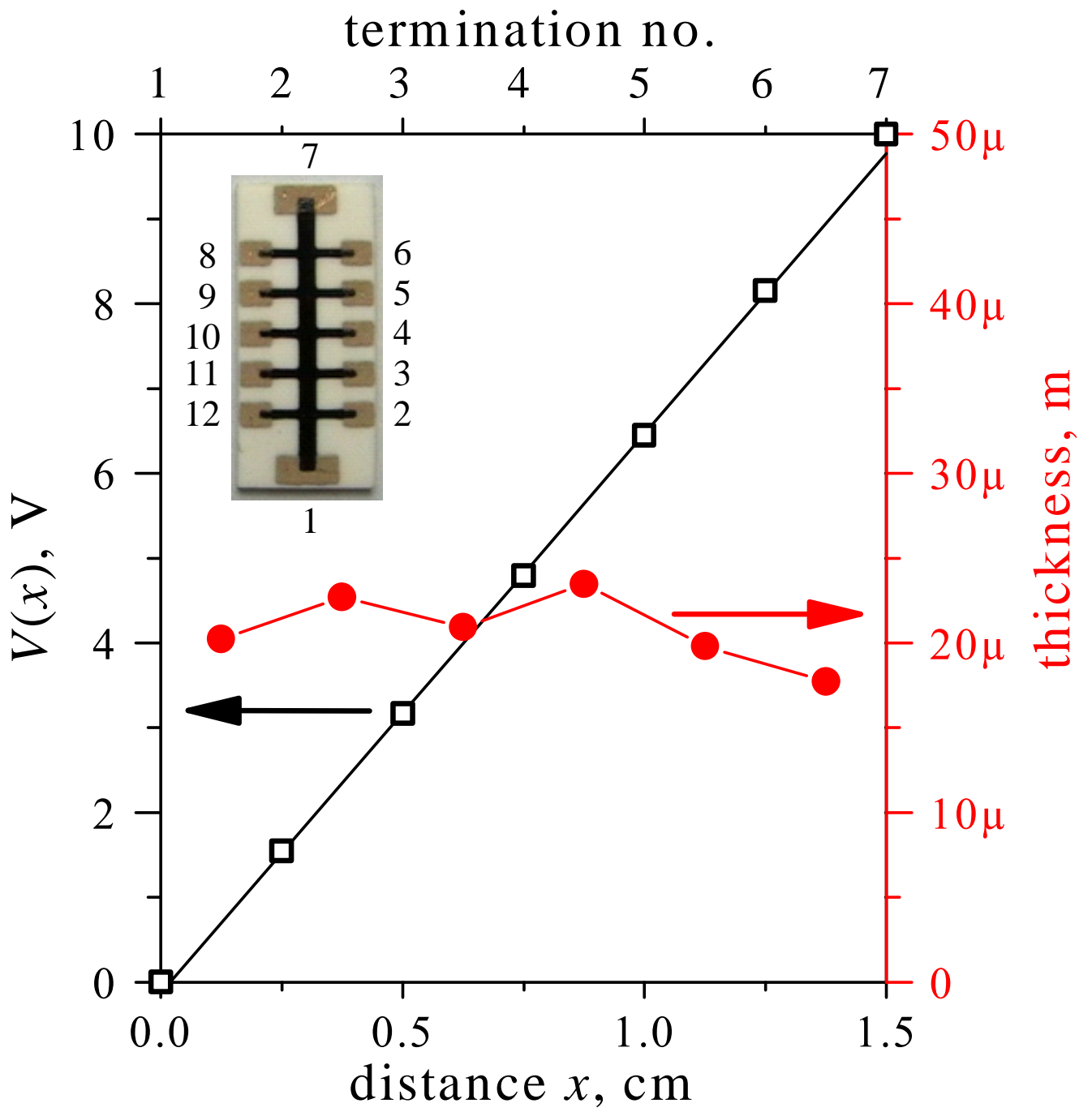


Figure 1 (figure1.eps)

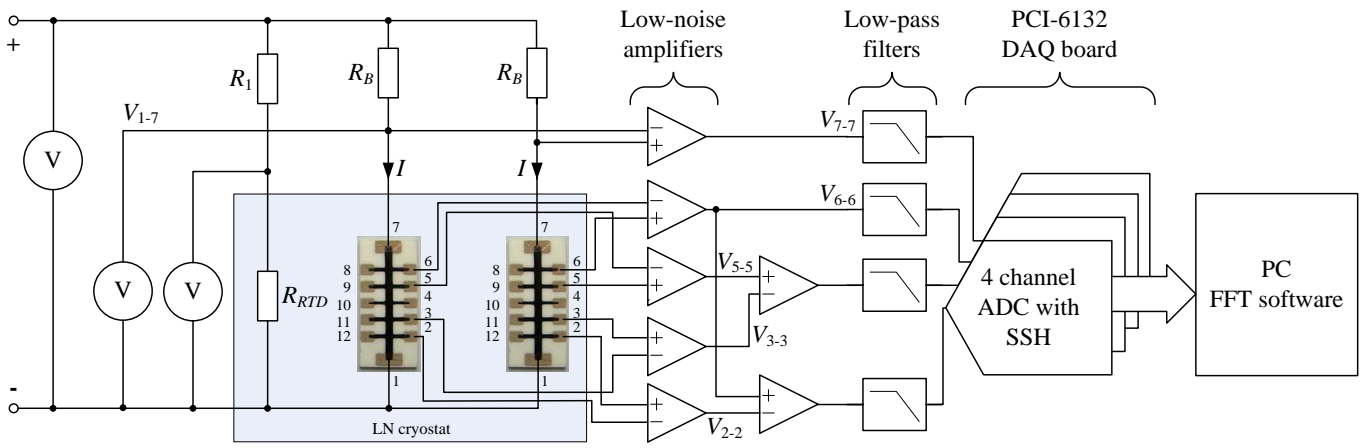


Figure 2 (figure2.eps)

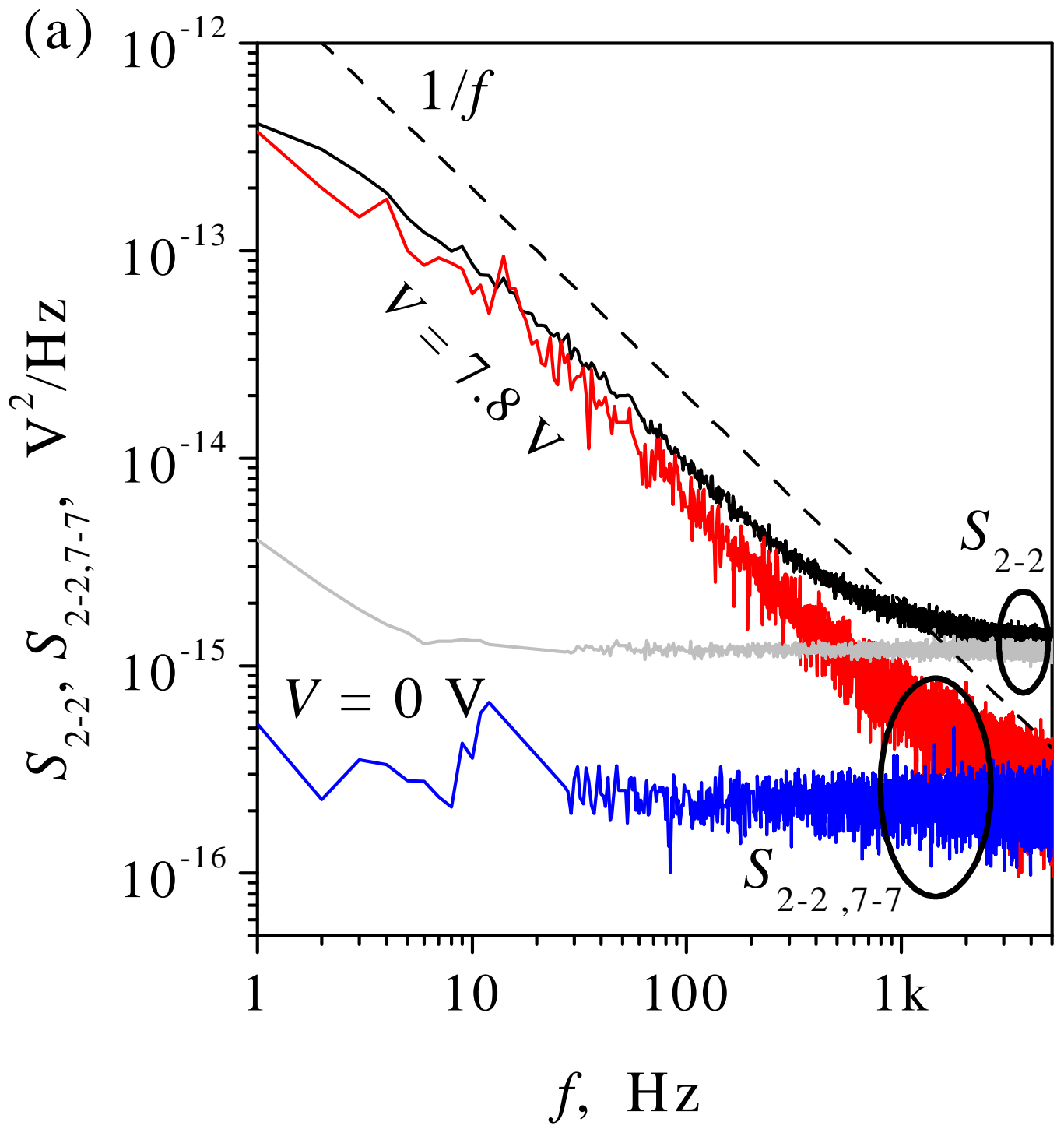


Figure 3a (figure3a.eps)

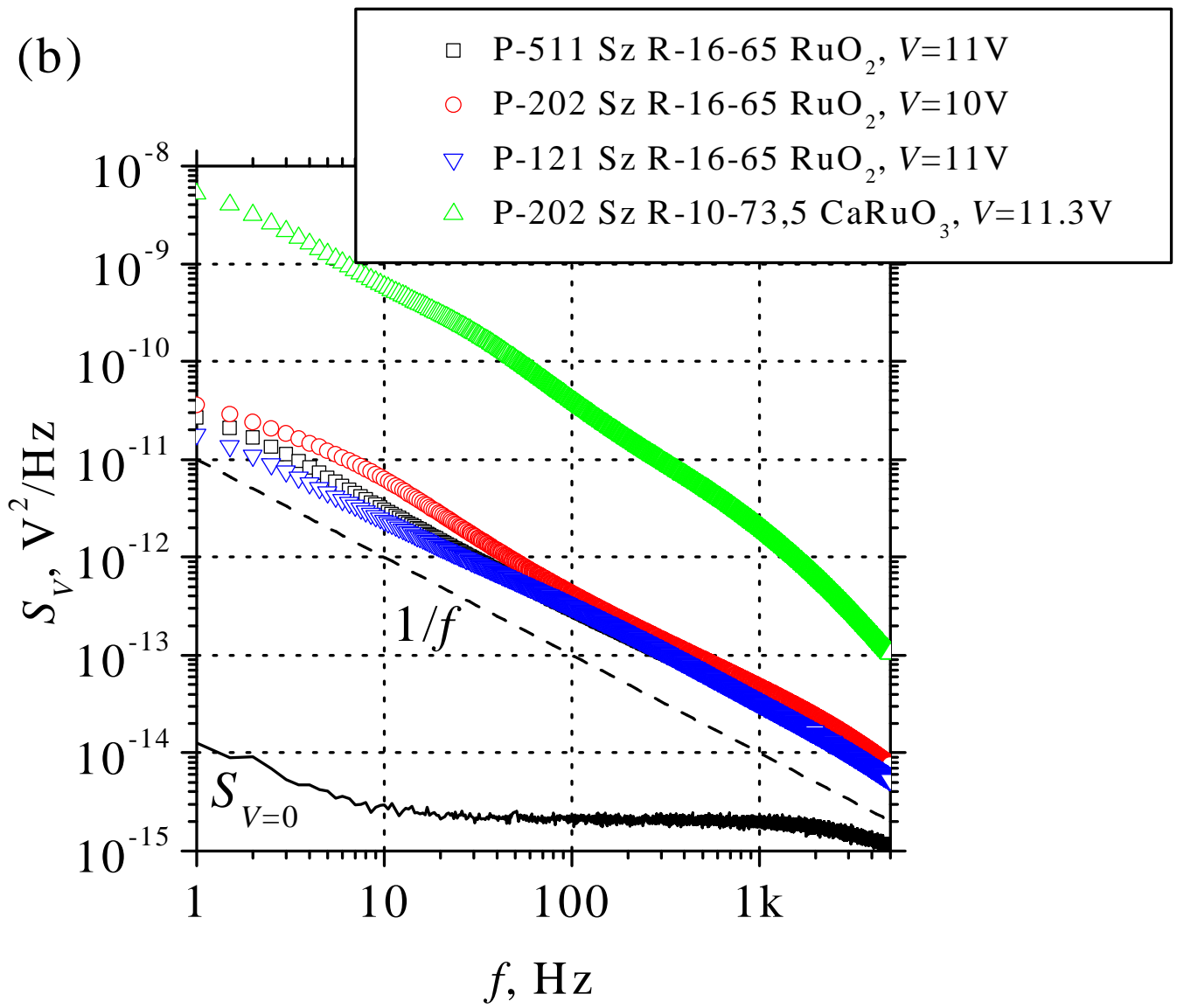


Figure 3b (figure3b.eps)

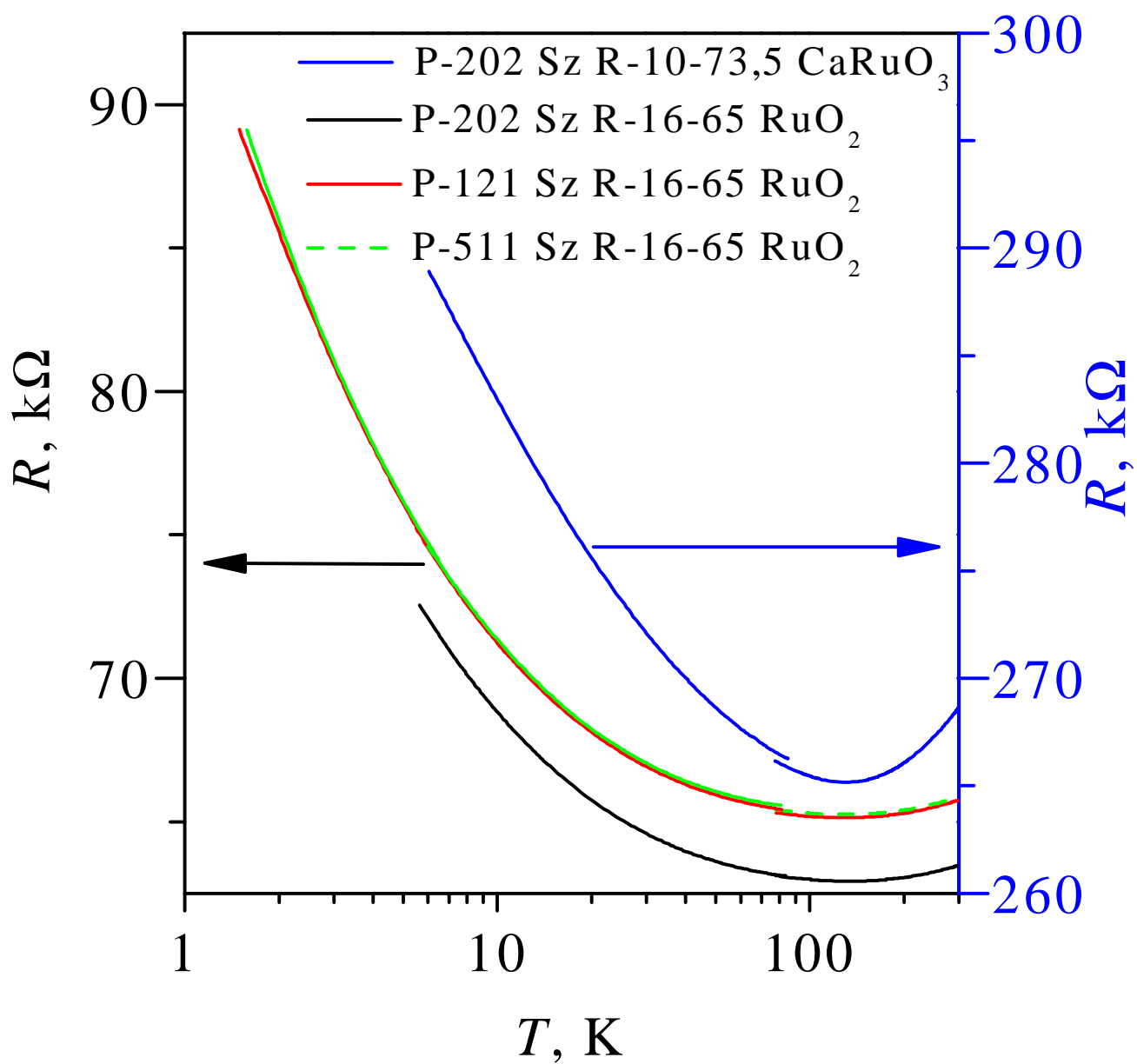


Figure 4 (figure4.eps)

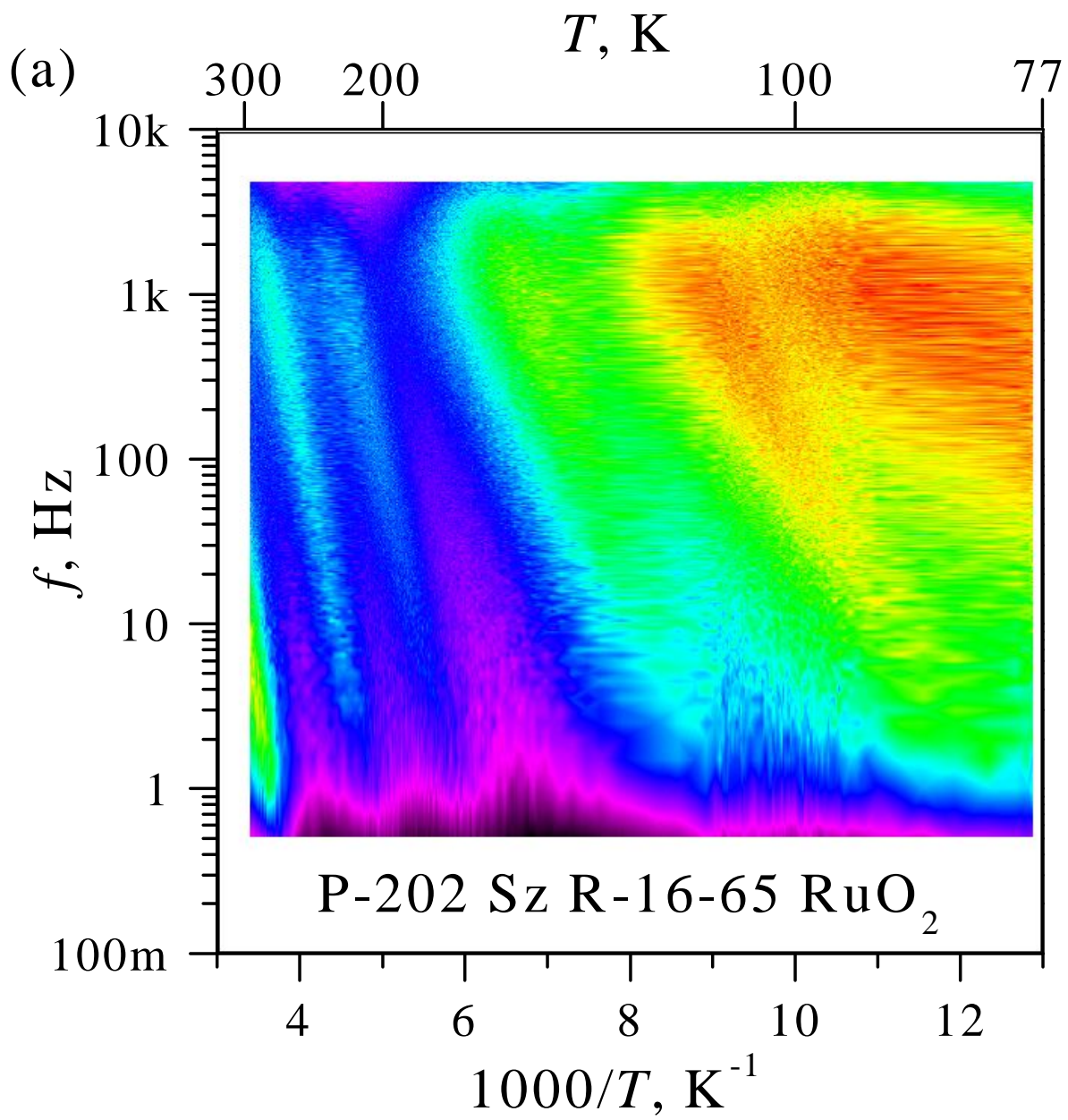


Figure 5a (figure5a.eps)

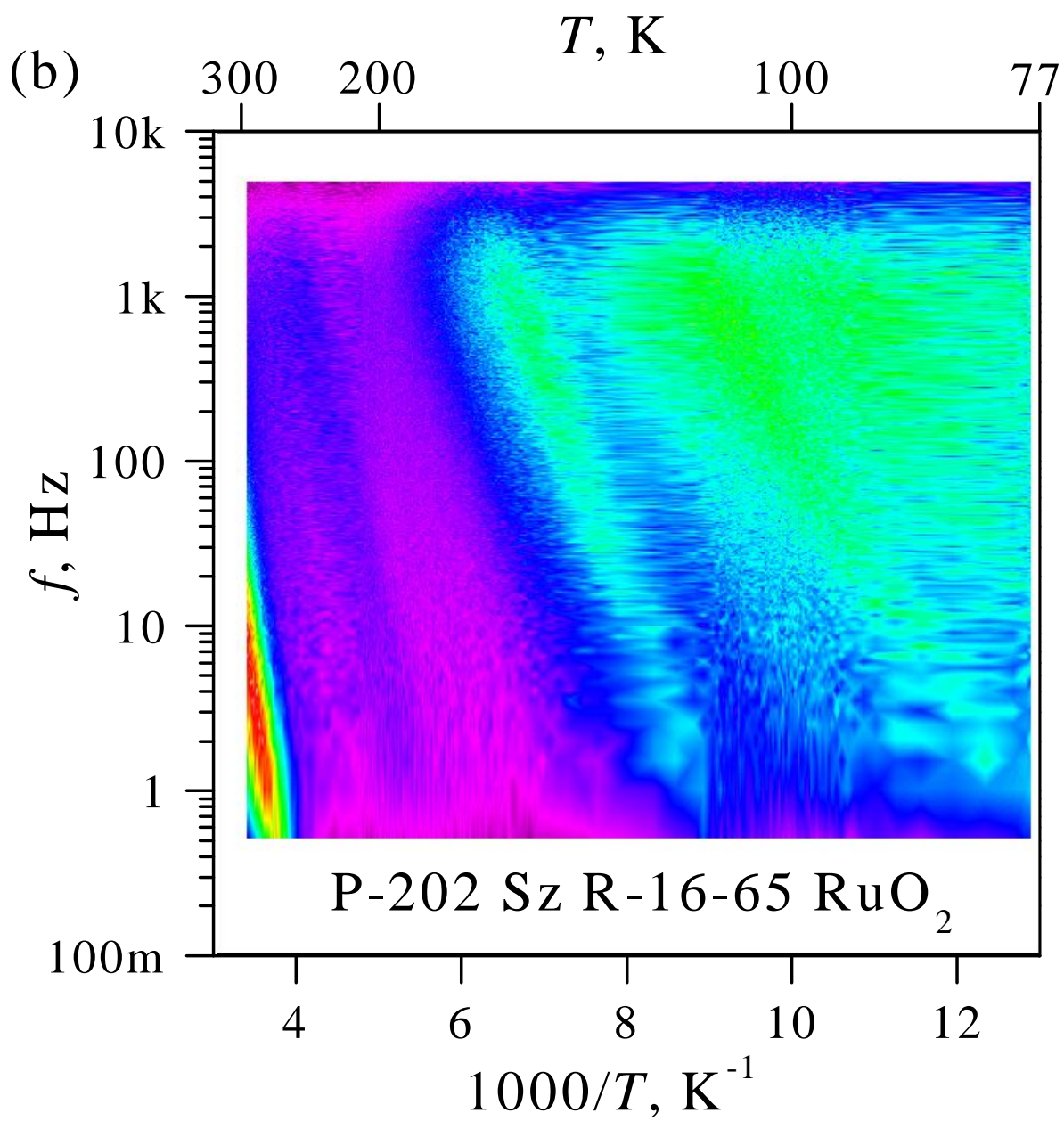


Figure 5b (figure5b.eps)

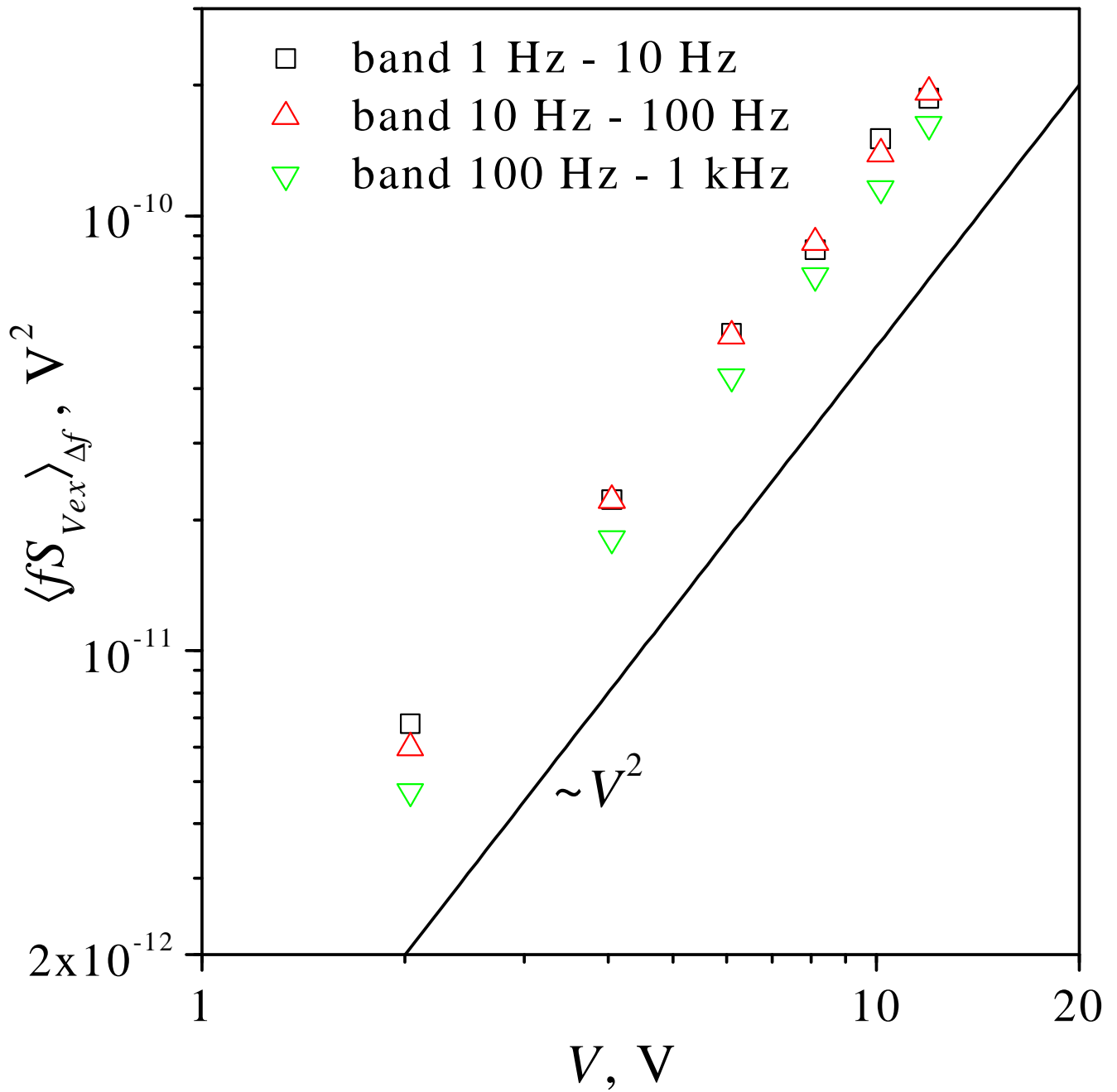


Figure 6 (figure6.eps)

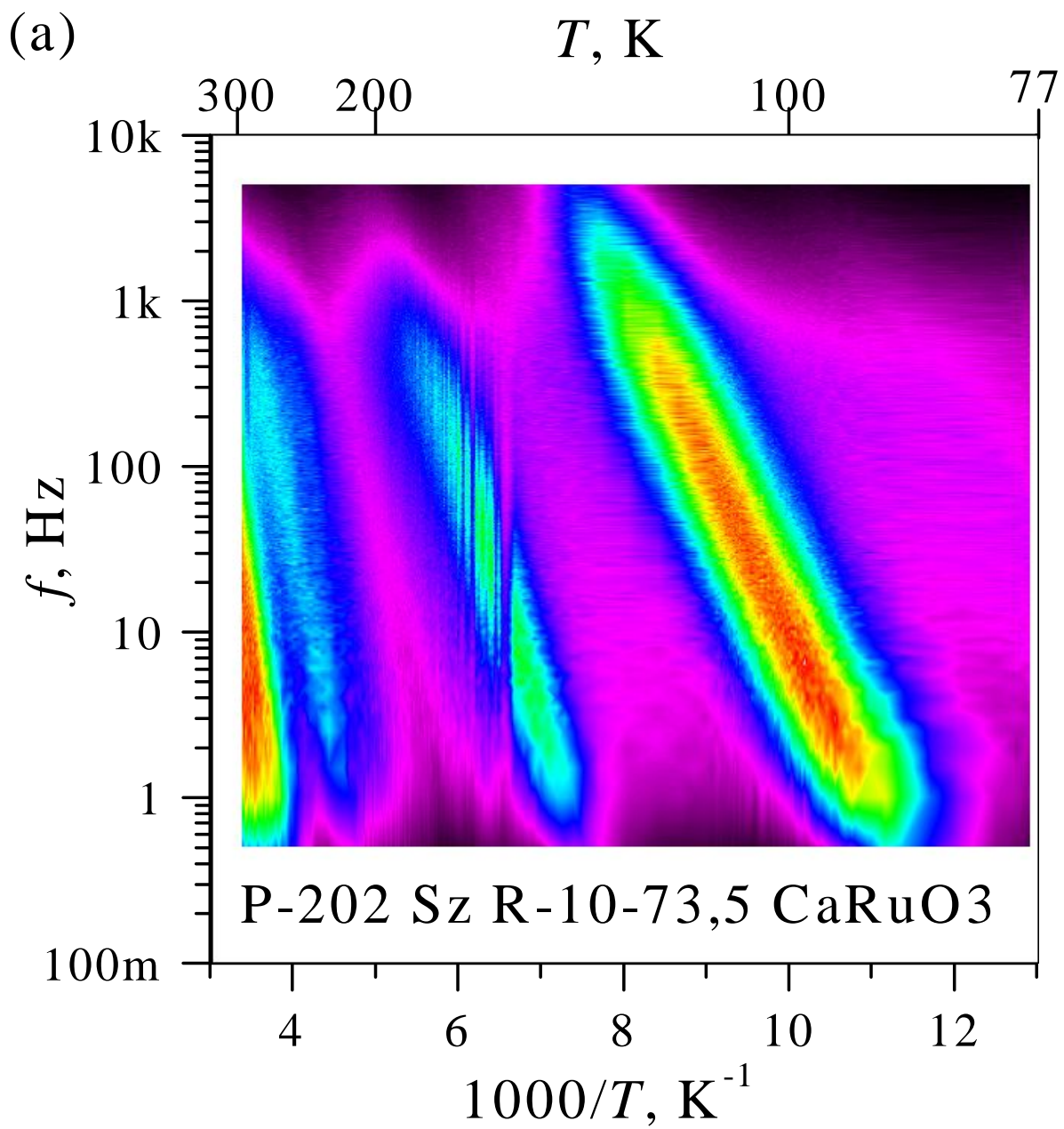


Figure 7a (figure7a.eps)

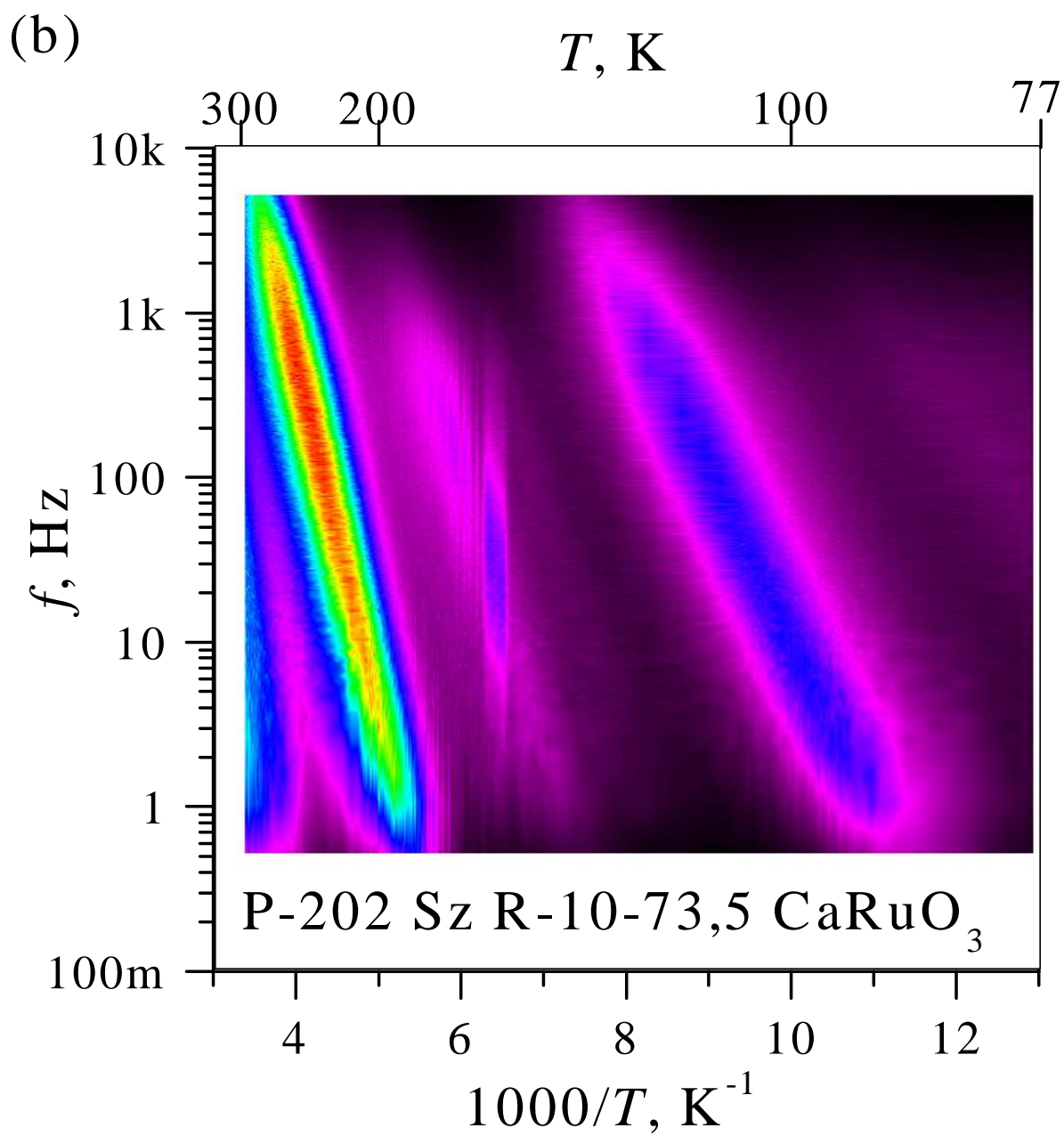


Figure 7b (figure7b.eps)

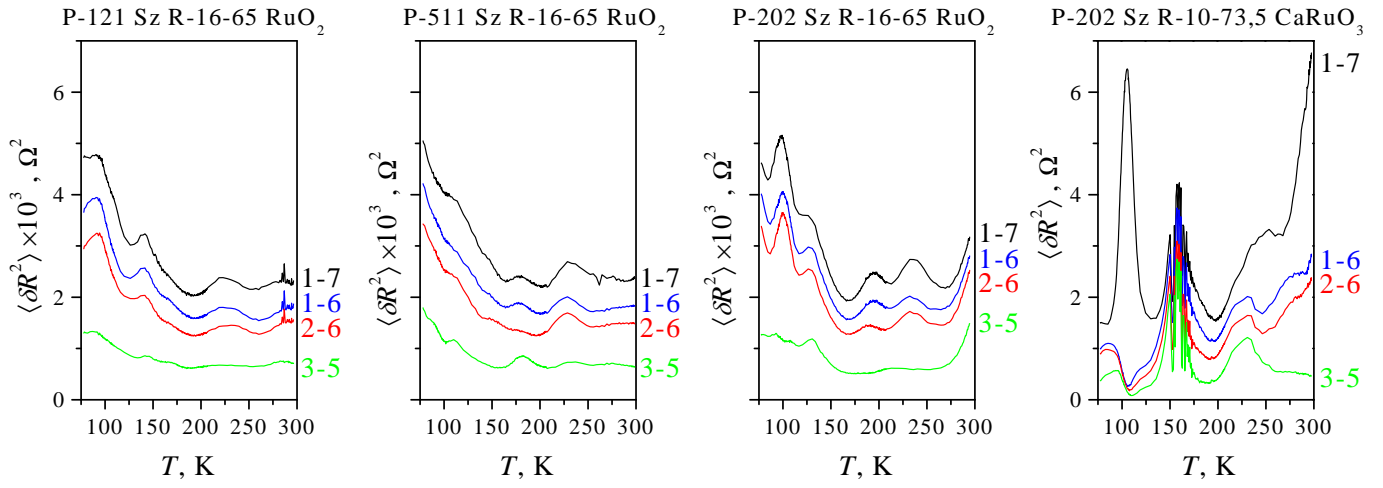


Figure 8 (figure8.eps)

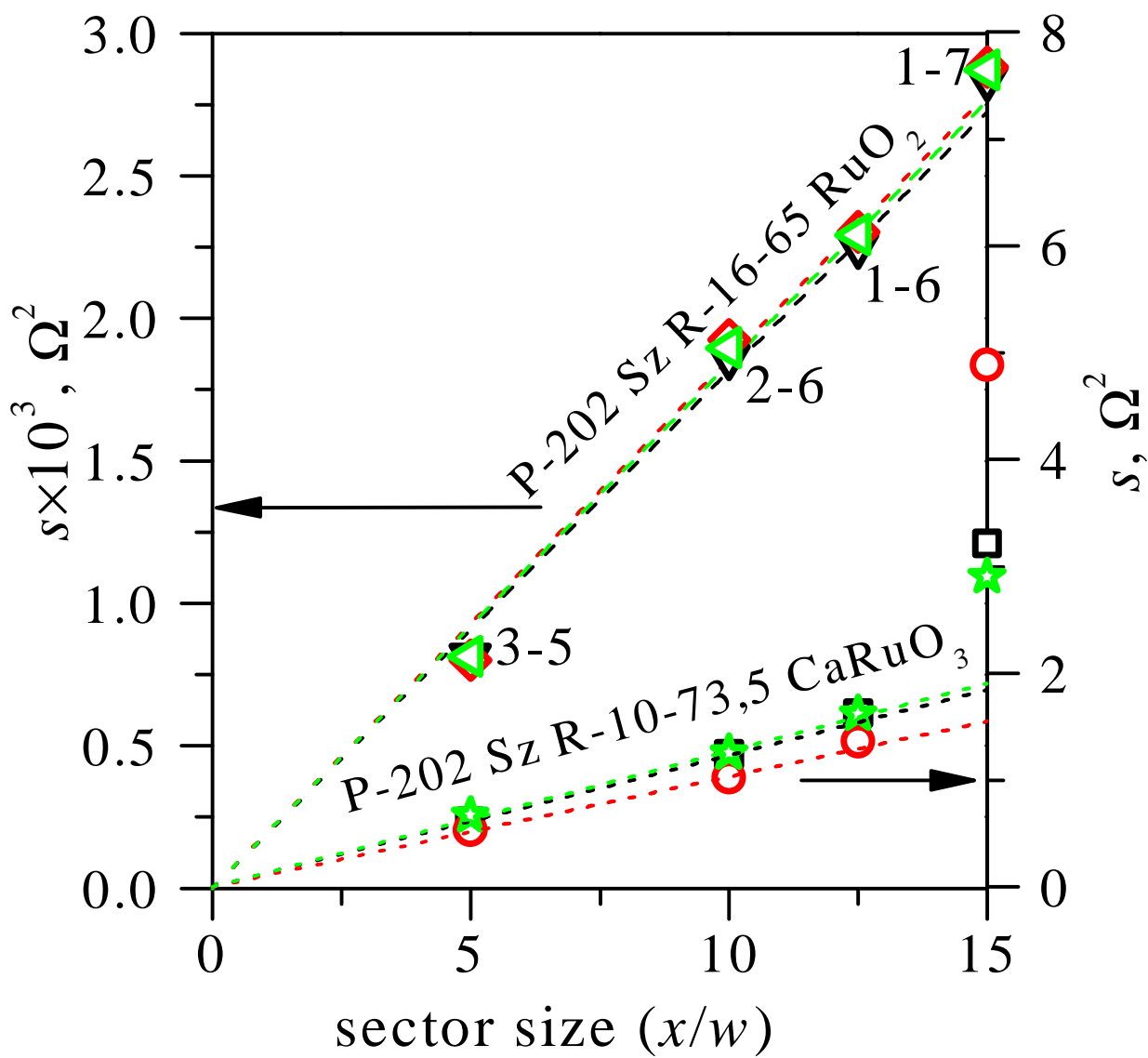


Figure 9 (figure9.eps)

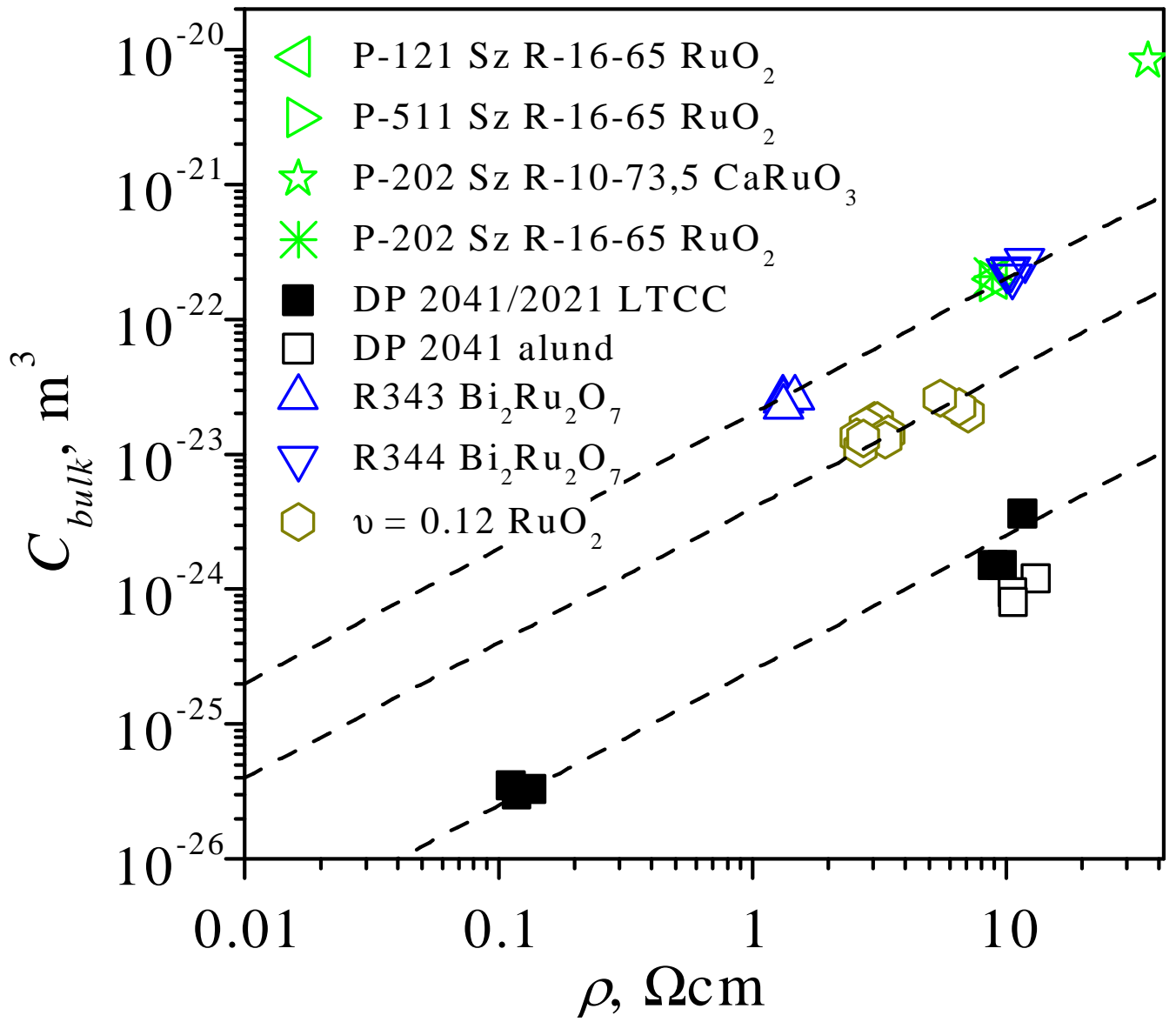


Figure 10 (figure10.eps)